

1 High-order cognition is supported by information-rich but  
2 compressible brain activity patterns

Lucy L. W. Owen<sup>1,2</sup> and Jeremy R. Manning<sup>1,\*</sup>

<sup>1</sup>Department of Psychological and Brain Sciences,  
Dartmouth College, Hanover, NH

<sup>2</sup>Carney Institute for Brain Sciences,  
Brown University, Providence, RI

\* Address correspondence to jeremy.r.manning@dartmouth.edu

March 14, 2023

### Abstract

We applied dimensionality reduction algorithms and pattern classifiers to functional neuroimaging data collected as participants listened to a story, temporally scrambled versions of the story, or underwent a resting state scanning session. These experimental conditions were intended to require different depths of processing and inspire different levels of cognitive engagement. We considered two primary aspects of the data. First, we treated the maximum achievable decoding accuracy across participants as an indicator of the “informativeness” of the recorded patterns. Second, we treated the number of features (components) required to achieve a threshold decoding accuracy as a proxy for the “compressibility” of the neural patterns (where fewer components indicate greater compression). Overall, we found that the peak decoding accuracy (achievable without restricting the numbers of features) was highest in the intact (unscrambled) story listening condition. However, the number of features required to achieve comparable classification accuracy was also lowest in the intact story listening condition. Taken together, our work suggests that our brain networks flexibly reconfigure according to ongoing task demands, and that the activity patterns associated with higher-order cognition and high engagement are both more informative and more compressible than the activity patterns associated with lower-order tasks and lower levels of engagement.

**Keywords:** information, compression, temporal decoding, dimensionality reduction, neuroimaging

## <sup>24</sup> Introduction

25 Large-scale networks, including the human brain, may be conceptualized as occupying one or  
26 more positions along on a continuum. At one extreme, every node is fully independent from  
27 every other node. At the other extreme, all nodes behave identically. Each extreme optimizes  
28 key properties of how the network functions. When every node is independent, the network is

29 maximally *expressive*: if we define the network’s “state” as the activity pattern across its nodes, then  
30 every state is equally reachable by a network with fully independent nodes. On the other hand, a  
31 network of identically behaved nodes optimizes *robustness*: any subset of nodes may be removed  
32 from the network without any loss of function or expressive power, as long as any single node  
33 remains. Presumably, most natural systems tend to occupy positions between these extremes. We  
34 wondered: might the human brain reconfigure itself to be more flexible or more robust according  
35 to ongoing demands? In other words, might the brain reconfigure its connections or behaviors  
36 under different circumstances to change its position along this continuum?

37 Closely related to the above notions of expressiveness versus robustness are measures of  
38 how much *information* is contained in a given signal or pattern, and how *redundant* a signal  
39 is (Shannon, 1948). Formally, information is defined as the amount of uncertainty about a given  
40 variables’ outcomes (i.e., entropy), measured in *bits*, or the optimal number of yes/no questions  
41 needed to reduce uncertainty about the variable’s outcomes to zero. Highly complex systems with  
42 many degrees of freedom (i.e., high flexibility and expressiveness), are more information-rich than  
43 simpler or more constrained systems. The redundancy of a signal denotes the difference between  
44 how expressive the signal *could* be (i.e., proportional to the number of unique states or symbols  
45 used to transmit the signal) and the actual information rate (i.e., the entropy of each individual  
46 state or symbol). If a brain network’s nodes are fully independent, then the number of bits required  
47 to express a single activity pattern is proportional to the number of nodes. The network would  
48 also be minimally redundant, since the status of every node would be needed to fully express a  
49 single brain activity pattern. If a brain network’s nodes are fully coupled and identical, then the  
50 number of bits required to express a single activity pattern is proportional to the number of unique  
51 states or values any individual node can take on. Such a network would be highly redundant,  
52 since knowing any individual node’s state would be sufficient to recover the full-brain activity  
53 pattern. Highly redundant systems are also robust, since there is little total information loss due  
54 to removing any given observation.

55 We take as a given that brain activity is highly flexible: our brains can exhibit nearly infinite ac-  
56 tivity patterns. This flexibility implies that our brains activity patterns are highly information rich.  
57 However, brain activity patterns are also highly structured. For example, full-brain correlation  
58 matrices are stable within (Finn et al., 2017, 2015; Gratton et al., 2018) and across (Cole et al., 2014;

59 Glerean et al., 2012; Gratton et al., 2018; Yeo et al., 2011) individuals. This stability suggests that  
60 our brains' activity patterns are at least partially constrained, for example by anatomical, external,  
61 or internal factors. Constraints on brain activity that limit its flexibility decrease expressiveness  
62 (i.e., its information rate). However, constraints on brain activity also increase its robustness to  
63 noise (e.g., “missing” or corrupted signals may be partially recovered). For example, recent work  
64 has shown that full-brain activity patterns may be reliably recovered from only a relatively small  
65 number of implanted electrodes (Owen et al., 2020; Scangos et al., 2021). This robustness property  
66 suggests that the relevant signal (e.g., underlying factors that have some influence over brain  
67 activity patterns) are compressible.

68 To the extent that brain activity patterns contain rich task-relevant information, we should  
69 be able to use the activity patterns to accurately differentiate between different aspects of the  
70 task (e.g., using pattern classifiers; Norman et al., 2006). For example, prior work has shown a direct  
71 correspondence between classification accuracy and the information content of a signal (Alvarez,  
72 2002). To the extent that brain activity patterns are compressible, we should be able to generate  
73 simplified (e.g., lower dimensional) representations of the data while still preserving the relevant  
74 or important aspects of the original signal. In general, information content and compressibility are  
75 related but are partially dissociable (Fig. 1). If a given signal (e.g., a representation of brain activity  
76 patterns) contains more information about ongoing cognitive processes, then the peak decoding  
77 accuracy should be high. And if the signal is compressible, a low-dimensional embedding of the  
78 signal will be similarly informative to the original signal (Fig. 1D).

79 Several recent studies suggest that the complexity of brain activity is task-dependent, whereby  
80 simpler tasks with lower cognitive demands are reflected by simpler and more compressible brain  
81 activity patterns, and more complex tasks with higher cognitive demands are reflected by more  
82 complex and less compressible brain activity patterns (Mack et al., 2020; Owen et al., 2021). These  
83 findings complement other work suggesting that functional connectivity (correlation) patterns are  
84 task-dependent (Cole et al., 2014; Finn et al., 2017; Owen et al., 2020), although see Gratton et  
85 al. (2018). Higher-order cognitive processing of a common stimulus also appears to drive more  
86 stereotyped task-related activity and functional connectivity across individuals (Hasson et al.,  
87 2008; Lerner et al., 2011; Simony & Chang, 2020; Simony et al., 2016).

88 The above studies are consistent with two potential descriptions of how cognitive processes are

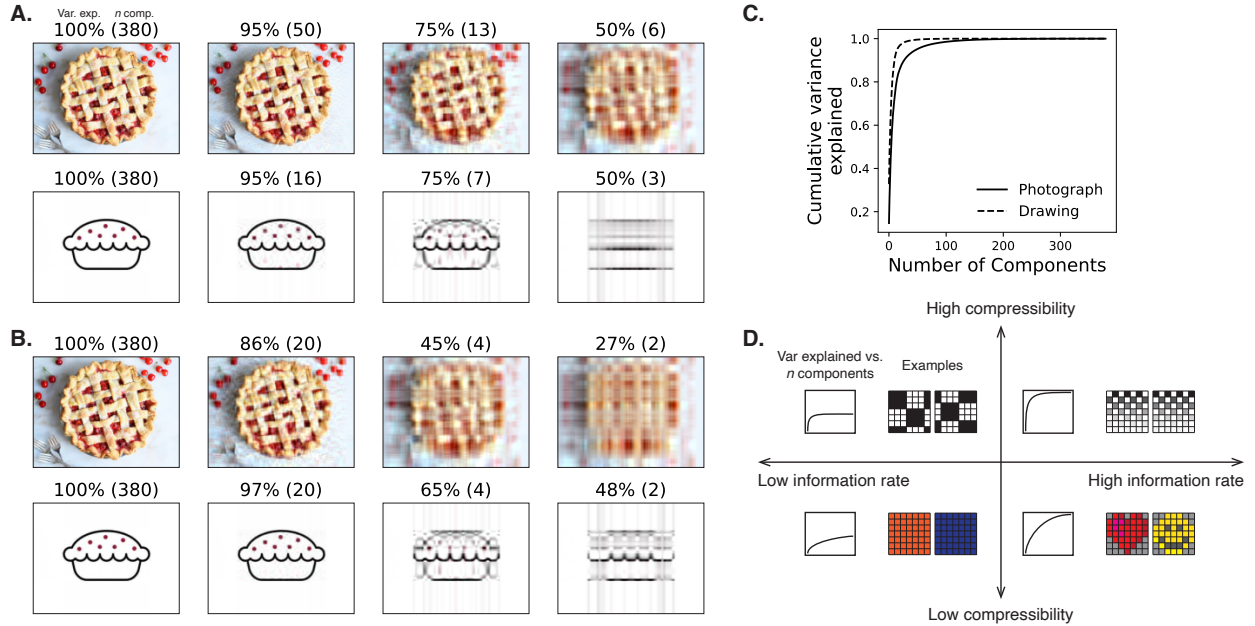


**Figure 1: Information content and compressibility.** **A. Variance explained for two images.** We applied principal components analysis to a photograph and drawing, treating the rows of the images as “observations.” Across columns, we identified the numbers of components required to explain 100%, 95%, 75%, or 50% of the cumulative variance in each image (the 100% columns denote the original images). The numbers of components are indicated in parentheses, and the resulting “compressed” images are displayed. **B. Representing two images with different numbers of components.** Using the same principal component decompositions as in Panel A, we computed the cumulative proportion of variance explained with 380 (original images), 20, 4, or 2 components. **C. Cumulative variance explained versus number of components.** For the images displayed in Panels A and B, we plot the cumulative proportion of variance explained as a function of the number of components used to represent each image. **D. Information rate and compressibility.** Across multiple images, the information rate (i.e., the amount of information contained in each image; horizontal axis) is high when each individual pixel provides information that cannot be inferred from other pixels. High-information rate images tend to be high-resolution, and low-information rate images tend to be low-resolution. Compressibility is related to the difference between the information required to specify the original versus compressed images (vertical axis). Highly compressible images often contain predictable structure (redundancies) that can be leveraged to represent the images much more efficiently than in their original feature spaces.

89 reflected in brain activity patterns. One possibility is that the information rate of brain activity in-  
90 creases during more complex or higher-level cognitive processing. If so, then the ability to reliably  
91 decode cognitive states from brain activity patterns should improve with task complexity or with  
92 the level (or “depth”) of cognitive processing. A second possibility is that the compressibility of  
93 brain activity patterns increases during more complex or higher-level cognitive processing. If so,  
94 then individual features of brain recordings, or compressed representations of brain recordings,  
95 should carry more information during complex or high-level (versus simple or low-level) cognitive  
96 tasks.

97 We used a previously collected neuroimaging dataset to estimate the extent to which each of  
98 these two possibilities might hold. The dataset we examined comprised functional magnetic reso-  
99 nance imaging (fMRI) data collected as participants listened to an audio recording of a 10-minute  
100 story, temporally scrambled recordings of the story, or underwent a resting state scan (Simony  
101 et al., 2016). Each of these experimental conditions evokes different depths of cognitive process-  
102 ing (Hasson et al., 2008; Lerner et al., 2011; Owen et al., 2021; Simony et al., 2016). We used  
103 across-participant classifiers to decode listening times in each condition, as a proxy for how “in-  
104 formative” the task-specific activity patterns were (Simony & Chang, 2020). We also use principle  
105 components analysis to generate lower-dimensional representations of the activity patterns. We  
106 then repeated the classification analyses after preserving different numbers of components and  
107 examined how classification accuracy changed across the different experimental conditions.

## 108 Results

109 We sought to understand whether higher-level cognition is reflected by more reliable and in-  
110 formative brain activity patterns, and how compressibility of brain activity patterns relates to  
111 cognitive complexity. We developed a computational framework for systematically assessing the  
112 informativeness and compressibility of brain activity patterns recorded under different cognitive  
113 circumstances. We used across-participant decoding accuracy (see *Forward inference and decoding*  
114 *accuracy*) as a proxy for informativeness. To estimate the compressibility of the brain patterns, we  
115 used group principal components analysis (PCA) to project the brain patterns into  $k$ -dimensional  
116 spaces, for different values of  $k$  (see *Hierarchical Topographic Factor Analysis (HTFA)* and *Principal*

117 components analysis (PCA)). For more compressible brain patterns, decoding accuracy should be  
118 more robust to small values of  $k$ .

119 We analyzed a dataset collected by Simony et al. (2016) that comprised four experimental  
120 conditions. These conditions exposed participants to stimuli that systematically varied in cognitive  
121 engagement. In the *intact* experimental condition, participants listened to an audio recording of  
122 a 10-minute story. In the *paragraph*-scrambled experimental condition, participants listened to a  
123 temporally scrambled version of the story, where the paragraphs occurred out of order, but where  
124 the same set of paragraphs was presented over the entire listening interval. All participants in  
125 this condition experienced the scrambled paragraphs in the same order. In the *word*-scrambled  
126 experimental condition, participants listened to a temporally scrambled version of the story, where  
127 the words occurred in a random order. Again, all participants in this condition experienced the  
128 scrambled words in the same order. Finally, in the *rest* experimental condition, participants lay  
129 in the scanner with no overt stimulus, while keeping their eyes open and blinking as needed.  
130 This public dataset provided a convenient means for testing our hypothesis that different levels  
131 of cognitive processing and engagement affect how informative and compressible the associated  
132 brain patterns are.

133 To evaluate the relation between informativeness and compressibility for brain activity from  
134 each experimental condition, we trained a series of across-participant temporal decoders on com-  
135 pressed representations of the data. Figure 2A displays the decoding accuracy as a function of the  
136 number of principal components used to represent the data. Several patterns were revealed by  
137 the analysis. First, in general (i.e., across experimental conditions), decoding accuracy improves  
138 as the number of components increases. However, decoding accuracy peaked at higher levels for  
139 experimental conditions that exposed participants to cognitively richer stimuli. The peak decoding  
140 accuracy was highest for the “intact” condition (versus paragraph:  $t(99) = 35.205, p < 0.001$ ; versus  
141 word:  $t(99) = 43.172, p < 0.001$ ; versus rest:  $t(99) = 81.361, p < 0.001$ ), next highest for the “para-  
142 graph” condition (versus word:  $t(99) = 6.243, p < 0.001$ ; versus rest:  $t(99) = 50.748, p < 0.001$ ),  
143 and next highest for the “word” condition (versus rest:  $t(99) = 48.791, p < 0.001$ ). This ordering  
144 implies that cognitively richer conditions evoke more stable brain activity patterns across people.

145 The cognitively richer conditions also displayed steeper initial slopes. For example, the intact  
146 condition decoders reached an arbitrarily chosen threshold of 5% accuracy using fewer components

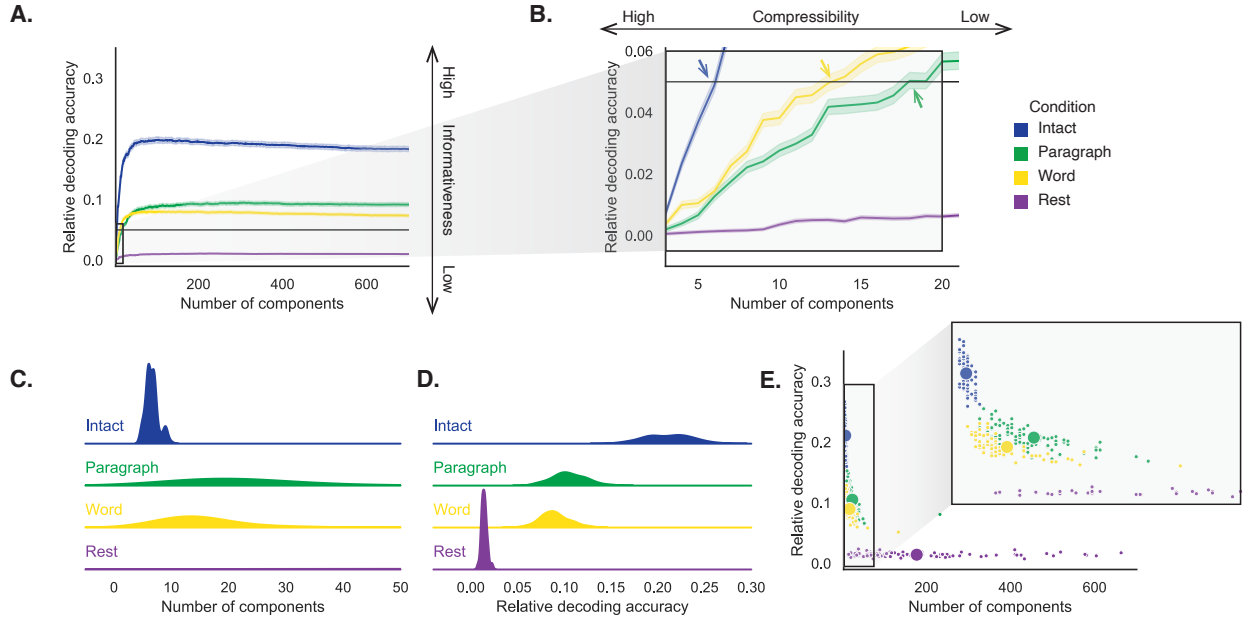


**Figure 2: Decoding accuracy and compression.** **A. Decoding accuracy by number of components.** Ribbons of each color display cross-validated decoding performance for each condition (intact, paragraph, word, and rest), as a function of the number of components (features) used to represent the data. For each condition, decoding accuracy has been normalized by subtracting expected “chance” decoding performance (estimated as  $\frac{1}{T}$ , where  $T$  is the number of timepoints in the given condition). This normalization was intended to enable fairer comparisons across conditions; a relative decoding accuracy of 0.0 denotes “chance” performance. The horizontal black line denotes 5% decoding accuracy (used as a reference in Panel B). **B. Numbers of components required to reach a fixed decoding accuracy threshold, by condition.** The panel displays a zoomed-in view of the inset in Panel A. Intersections between each condition’s decoding accuracy curve and the 5% decoding accuracy reference line are marked by arrows. All error ribbons in Panels A and B denote bootstrap-estimated 95% confidence intervals. **C. Estimating “compressibility” for each condition.** The density plots display the numbers of components required to reach at least 5% (corrected) decoding accuracy, across all cross validation runs. For the “rest” condition, where decoding accuracy never reached 5% accuracy, we display the distribution of the numbers of components required to achieve the peak decoding accuracy in each fold. (This distribution is nearly flat, as illustrated in Panel E.) **D. Estimating “informativeness” for each condition.** The density plots display the peak (corrected) decoding accuracies achieved in each condition, across all cross validation runs. **E. Informativeness versus compressibility.** Each dot displays the minimum number of components required to achieve at least 5% corrected decoding accuracy ( $x$ -coordinate; for the rest condition the numbers of components are estimated using the peak decoding accuracies as in Panel C) and the peak (corrected) decoding accuracy ( $y$ -coordinate). The smaller dots correspond to individual cross validation runs and the larger dots display the averages across runs. The inset displays a zoomed-in view of the indicated region in the main panel.

147 than the paragraph condition decoders ( $t(99) = -7.429, p < 0.001$ ) or word condition decoders  
148 ( $t(99) = -7.300, p < 0.001$ ), and decoding accuracy never exceeded 5% for the rest condition. This  
149 suggests that brain activity patterns evoked by cognitively richer conditions are more compressible,  
150 such that representing the data using the same number of principal components provides more  
151 information to the temporal decoders (Fig. 2B).

152 In every experimental condition, decoding accuracy appeared to asymptote (i.e., hit an upper  
153 limit) beyond some characteristic number of components that differed across conditions. To  
154 quantify the “inflection points” at which the decoding curves in Figure 2A flattened out, we fit a  
155 sigmoid function to the average decoding curve for each condition. We defined the inflection point  
156 for each condition as the point on the fitted sigmoid where the second derivative was both positive  
157 and less than a threshold value of 0.0001 (i.e., approaching 0 from the right). These inflection  
158 points reflect a “balance” between higher decoding accuracy (which tends to be better when  
159 more components are used) and compression (which is better for fewer components). Plotting  
160 each condition’s inflection point (Fig. 2D) reveals that both the number of components and the  
161 decoding accuracy at each inflection point increase systematically across conditions in proportion  
162 to cognitive richness.

163 If informativeness (to the temporal decoders) and compressibility vary with the cognitive  
164 richness of the stimulus, might these measures also vary over time *within* a given condition? For  
165 example, participants in the intact condition might process the ongoing story more deeply later  
166 on in the story (compared with earlier in the story) given the additional narrative background  
167 and context they had been exposed to by that point. To examine this possibility, we divided  
168 each condition into three successive time segments. We computed decoding curves (Fig. 3A)  
169 and inflection points (Fig. 3B) for each segment and condition. We found that, in the two most  
170 cognitively rich conditions (intact and paragraph), both decoding accuracy and compressibility,  
171 as reflected by the change in decoding curves, increased with listening time (e.g., at the annotated  
172 reference point of  $k = 20$  components: intact:  $t(99) = 7.915, p < 0.001$ ; paragraph:  $t(99) =$   
173  $2.354, p = 0.021$ ). These changes may reflect an increase in comprehension or depth of processing  
174 with listening time. In contrast, the decoding accuracy and compressibility *decreased* with listening  
175 time in the word condition ( $t(99) = -10.747, p < 0.001$ ) and rest condition ( $t(99) = -22.081, p <$   
176  $0.001$ ). This might reflect the depletion of attentional resources in the less-engaging word and rest

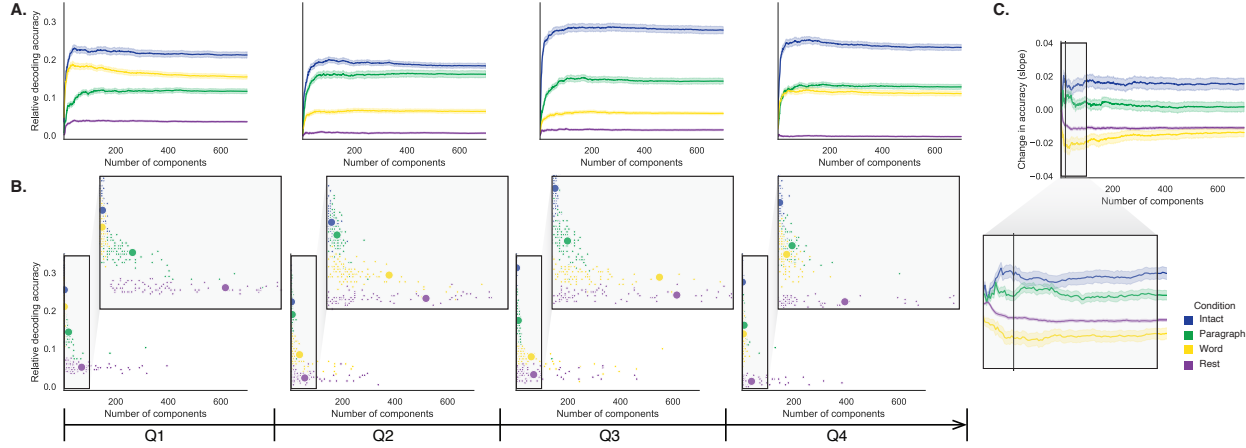


**Figure 3: Changes in decoding accuracy and compression over time.** **A. Decoding accuracy by number of components, by story segment.** Each family of curves is plotted in the same format as Figure 2A but reflects data only from one quarter of the dataset. **B. Informativeness versus compressibility by condition and segment.** Each scatter plot is in the same format as Figure 2E, but reflects data only from one quarter of the dataset. **C. Change in decoding accuracy over time, by number of components.** For each number of components ( $x$ -axis) and condition (color), we fit a regression line to the decoding accuracies obtained for the first, second, third, and fourth quarters of the dataset (corresponding to the columns of Panels A and B). The  $y$ -axis denotes the slopes of the regression lines. All error ribbons denote bootstrap-estimated 95% confidence intervals.

177 conditions.

178 We also wondered how informativeness and compressibility in the different experimental  
 179 conditions might vary across brain networks. We used a network parcellation identified by  
 180 Yeo et al. (2011) to segment the brain into seven distinct networks. The networks can be sorted  
 181 (roughly) in order from lower-level to higher-level cortex as follows (Fig. 4A): visual, somatomotor,  
 182 dorsal attention, ventral attention, limbic, frontoparietal, and default mode. Next, we computed  
 183 decoding curves separately for the activity patterns within each network and identified each  
 184 network's inflection point, for each experimental condition. Moving from low-order networks  
 185 to higher-order networks, we found that decoding accuracy (for the intact condition) tended to  
 186 increase (Fig. 4B). This suggests that higher-order networks may carry more content-relevant or  
 187 stimulus-driven "information." We found no clear trends in the numbers of components at each  
 188 network's inflection point across networks or conditions (Fig. 4C).

189 In addition to examining different networks in isolation, we wondered about the general  
 190 structure of the full-brain (i.e., potentially multi-network) activity patterns reflected by different  
 191 principal components across different experimental conditions. Figure 5 displays inflated brain

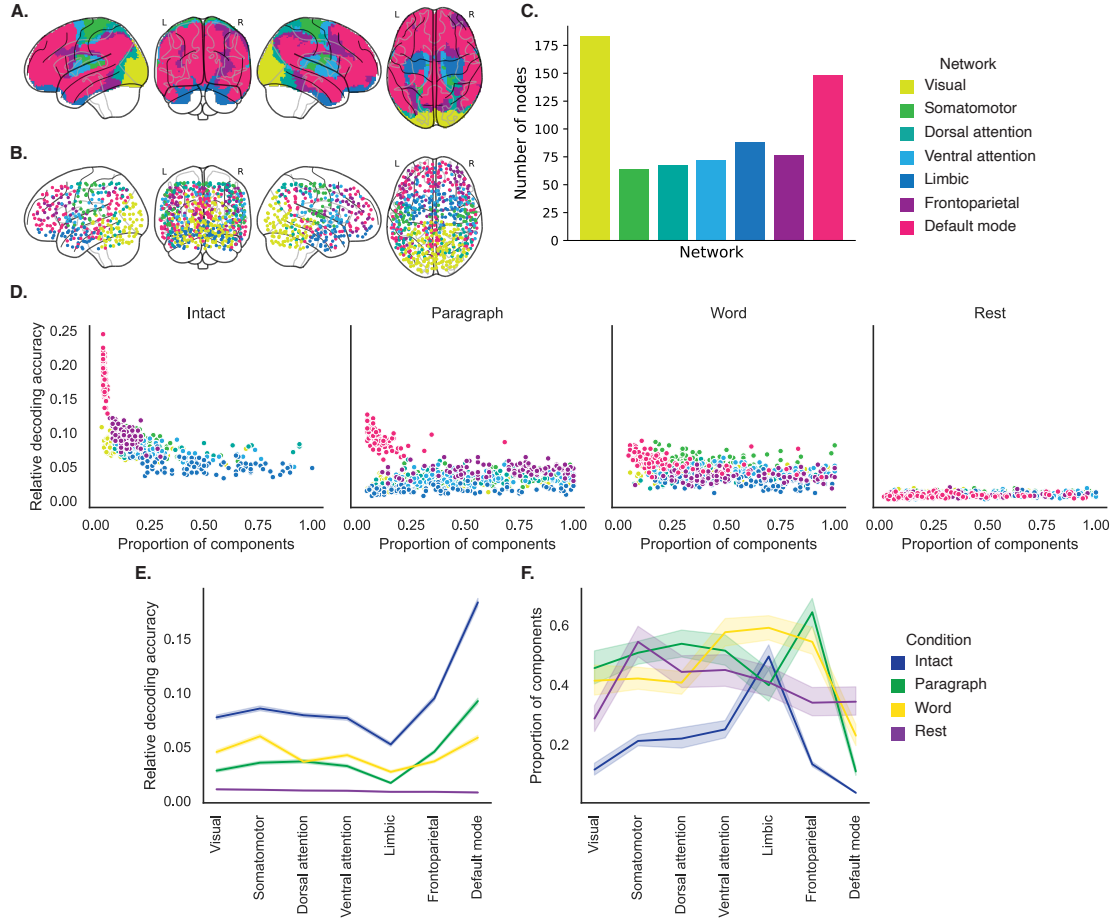


**Figure 4: Network-specific decoding accuracy and compression.** **A. Network parcellation map.** The glass brain displays the location of each of seven networks identified by Yeo et al. (2011). **B. Node labels.** We assigned network labels to each of 700 Hierarchical Topographic Factor Analysis-derived nodes (see *Hierarchical topographic factor analysis (HTFA)*). For each node, we evaluated its radial basis function (RBF) at the locations of every voxel in the parcellation map displayed in Panel A. We summed up these RBF weights separately for the voxels in each network. We defined each node's network label as its highest-weighted network across all voxels. **C. Per-network node counts.** The bar plot displays the total number of HTFA-derived nodes assigned to each network. **D. Informativeness versus compressibility by network and condition.** Each dot corresponds to a single cross validation run. The dots' coordinates denote the minimum proportion of components (relative to the number of nodes in the given network) required to achieve at least 5% corrected decoding accuracy ( $x$ -coordinate; for the rest condition these proportions are estimated using the peak decoding accuracies) and peak (corrected) decoding accuracy ( $y$ -coordinate). We repeated the analysis separately for each network (color) and experimental condition (column). **E. Informativeness by network.** For each network, sorted (roughly) from lower-order networks on the left to higher-order networks on the right, the curves display the peak (corrected) decoding accuracy for each experimental condition (color). **F. Compressibility by network.** For each network, the curves display the proportion of components (relative to the total possible number of components displayed in Panel C) required to achieve at least 5% decoding accuracy (or, for the rest condition, peak decoding accuracy, as described above). Error ribbons in Panels E and F denote 95% bootstrap-estimated confidence intervals.

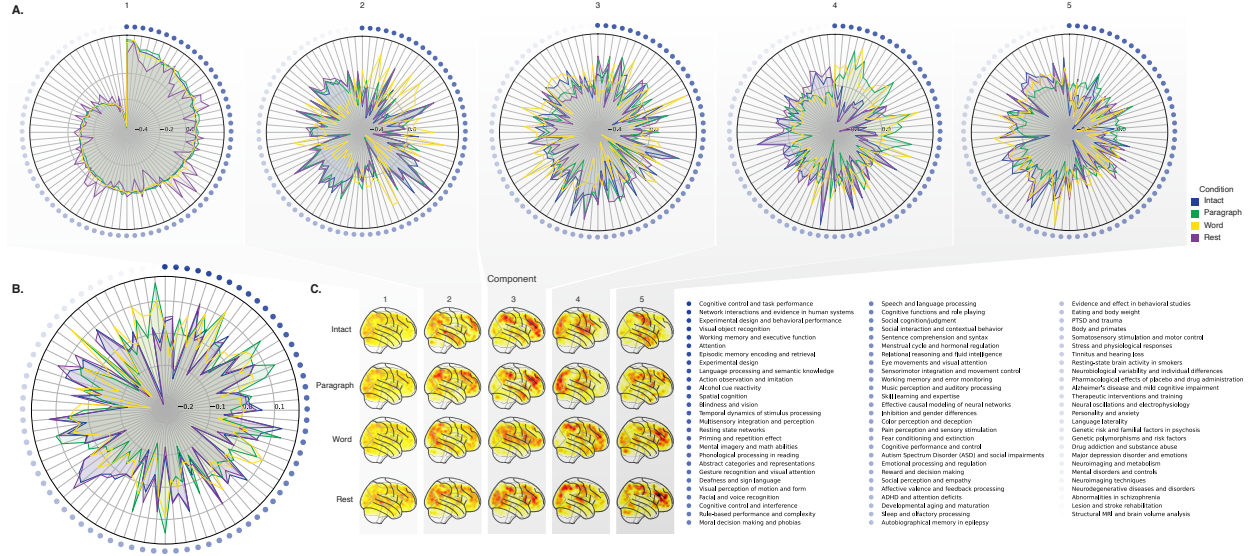


**Figure 5: Neurosynth topic weightings by component.** We used a reverse inference procedure (see *Reverse inference*) to estimate the correspondences between brain images and a set of 80 topics derived from the Neurosynth database of neuroimaging articles (Rubin et al., 2017). **A. Topic correlations by component.** For each of the top five highest-weighted principal components (columns) derived from each experimental condition (colors), the radar plots display the correlations between the component images and the per-topic images derived for each topic (topic identities are denoted by the blue dots; a legend for the topic labels is in the lower right of the figure). The top-weighted terms for each topic may be found in Table S1. **B. Topic correlations averaged across components.** The radar plot is in the same format as the plots in Panel A, but here we display the per-condition average correlations across the top five components (for each condition) reflected in Panel A. **C. Component images.** Each plot displays a right sagittal view of a glass brain projection of the top five principal components (columns) for each experimental condition (rows). Additional projections for each component may be found in Figure S4.

maps of the top five highest-weighted components, for each experimental condition. We also used Neurosynth (Rubin et al., 2017) to identify, for each component, the top five terms associated with each map (see *Reverse inference*). We noticed (by inspection) several common themes across the sets of terms associated with each component and condition. Memory-related components included terms like “middle temporal,” “memory retrieval,” and “working memory.” Sensory processing related components included terms like “primary visual,” “auditory cortex,” “v1,” and so on. Other components were associated with sensory integration (e.g., “thalamic,” “cingulate,” etc.), sentence comprehension (e.g., “sentence,” “comprehension”), emotion and valence (e.g., “amygdala,” “valance”), or the default mode network (e.g., “default mode”). The components we identified were relatively stable across story segments (Fig. S1).

## Discussion

We examined fMRI data collected as participants listened to an auditory recording of a story, scrambled recordings of the story, or underwent a resting state scan. We found that cognitively richer stimuli evoked more reliable (i.e., consistent across people) and information rich brain activity patterns. The brain patterns evoked by cognitively richer stimuli were also more compressible, in that each individual component provided more “signal” to temporal decoders relative to components of data from less cognitively rich conditions (Fig. 2). Over time (e.g., as the experiment progressed), these phenomena were strengthened. Specifically, across story segments, data from more cognitively rich conditions became more informative and compressible, and data from less cognitively rich conditions became *less* informative and compressible (Fig. 3). We also repeated these analyses separately for different brain networks. We found that networks traditionally associated with higher-level cognitive functions tended to provide more informative brain patterns than networks traditionally associated with lower level cognitive functions (Fig. 4). Finally, we examined the most dominant components of the brain activity patterns from each experimental condition. We used a reverse inference approach (Rubin et al., 2017) to identify the terms in the neuroimaging literature most commonly associated with the corresponding maps. As summarized in Figure 6, we found that terms associated with memory and sensory processing were associated with the strongest components in all three story listening conditions. Terms associated with sensory in-

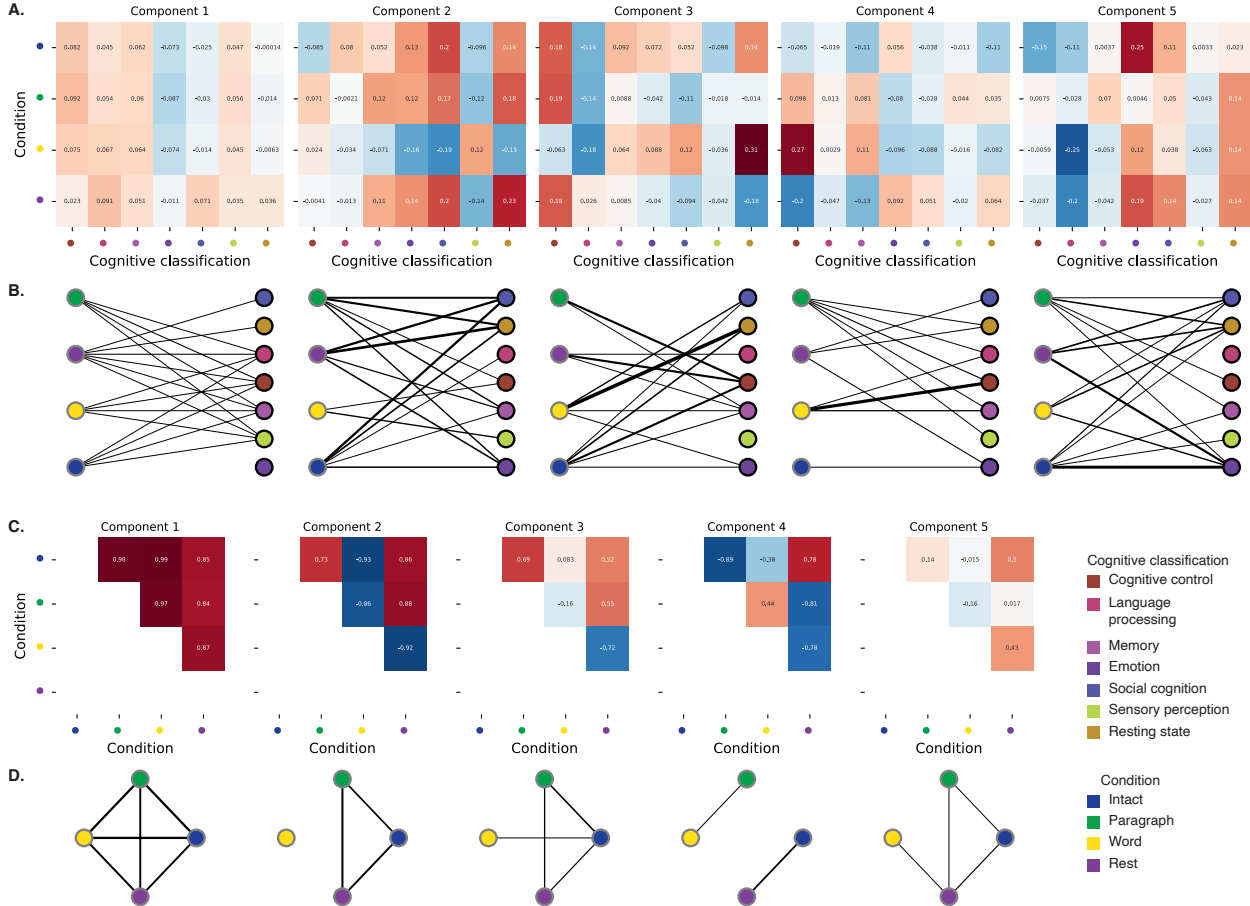


**Figure 6: Summary of functions associated with top-weighted components by condition. A. Top-weighted topics by condition.** Here we display per-condition (rows, indicated by colored dots) topic correlations, averaged across topics that pertain to each of several broad cognitive functions (columns within each sub-panel, indicated by colored dots). Each sub-panel reflects correlations for the components indicated in the panel titles. A legend for the condition and several core cognitive function classifications is displayed in the lower right of the figure. Table S1 provides a list of each topic's top-weighted terms, along with each topic's manually labeled cognitive classification. A full list of the topics most highly associated with each component may be found in Figure S5. **B. Associations between per-condition components and cognitive functions.** The network plots denote positive average correlations between the component images for each condition (gray-outlined dots on the left sides of each network; colors denote conditions) and topic-specific brain maps associated with each indicated cognitive function (black-outlined dots on the right sides of each network; colors denote cognitive functions). The line thicknesses are proportional to the correlation values (correlation coefficients are noted in the heatmaps in Panel A). **C. Correlations between each principal component, by condition.** The heatmaps display the correlations between the brain maps (Fig. S4) for each principal component (sub-panel), across each pair of conditions (rows and columns of each sub-panel's matrix, indicated by colored dots). **D. Associations between per-condition components, by component.** Each sub-panels network plot summarizes the pattern of correlations between the  $n^{\text{th}}$  top-weighted principal components (sub-panel) for each experimental condition (gray-outlined dots). The line thicknesses are proportional to the correlation values (correlation coefficients are noted in the heatmaps in Panel C).

220 tegration were associated with the strongest components in the intact and paragraph-scrambled  
221 conditions. Terms associated with sentence comprehension, emotion, and valence were associated  
222 with the strongest components in the intact condition. Finally, terms associated with the default  
223 mode network were associated with the strongest components in the word-scrambled and resting  
224 state conditions. Taken together, our findings indicate that the informativeness and compressibil-  
225 ity of our brain activity patterns are task-dependent, and these properties change systematically  
226 with factors like cognitive richness and depth of processing.

227 Our explorations of informativeness and compressibility are related to a much broader litera-  
228 ture on the correlational and causal structure of brain activity patterns (Adachi et al., 2012; Bassett  
229 & Sporns, 2017; Brovelli et al., 2004; Bullmore & Sporns, 2009; Dhamala et al., 2008; Korzeniewska  
230 et al., 2008; Owen et al., 2021; Preti et al., 2017; Rogers et al., 2007; Rubinov & Sporns, 2010; Size-  
231 more et al., 2018; Smith, Beckmann, et al., 2013; Smith, Vidaurre, et al., 2013; Sporns & Betzel, 2016;  
232 Sporns & Honey, 2006; Sporns & Zwi, 2004; Srinivasan et al., 2007; Tomasi & Volkow, 2011; Yeo  
233 et al., 2011). Correlations or causal associations between different brain regions simultaneously  
234 imply that full-brain activity patterns will be compressible and also that those activity patterns  
235 will contain redundancies. For example, the extent to which activity patterns at one brain area can  
236 be inferred or predicted from activity patterns at other areas (e.g., Owen et al., 2020; Scangos et al.,  
237 2021), reflects overlap in the information available in or represented by those brain areas. If brain  
238 patterns in one area are recoverable using brain patterns in another area, then the “signal” used to  
239 convey the activity patterns could be compressed by removing the recoverable activity. Predictable  
240 (and therefore redundant) brain activity patterns are also more robust to signal corruption. For  
241 example, even if the activity patterns at one region are unreadable or unreliable at a given moment,  
242 that unreliability could be compensated for by other regions’ activity patterns that were predictive  
243 of the unreliable region.

244 Our findings that informativeness and compressibility change with task demands may follow  
245 from task-dependent changes in full-brain correlation patterns. A number of prior studies have  
246 found that so-called “functional connectivity” (i.e., correlational) patterns vary reliably across  
247 tasks, events, and situations (Cole et al., 2014; Owen et al., 2021; Simony et al., 2016; Smith et  
248 al., 2009). By examining how these task-dependent changes in correlations affect informativeness  
249 and compressibility, our work suggests a potential reason why the statistical structure of brain

250 activity patterns might vary with cognitive task or with cognitive demands. For lower-level tasks,  
251 or for tasks that require relatively little “deep” cognitive processing, our brains may optimize  
252 activity patterns for robustness and redundancy over expressiveness, for example to maximize  
253 reliability. For higher-level tasks, or for tasks that require deeper cognitive processing, our brains  
254 may sacrifice some redundancy in favor of greater expressiveness.

255 In the information theory sense (Shannon, 1948), when a signal is transmitted using a fixed  
256 alphabet of “symbols,” the information rate decreases as the signal is compressed (e.g., fewer sym-  
257 bols transmitted per unit time, using an alphabet with fewer symbols, etc.). Our finding that each  
258 individual brain component (symbol) becomes more informative as cognitive richness increases  
259 suggests that the “alphabet” of brain activity patterns is also task-dependent. Other work suggests  
260 that the representations that are *reflected* by brain activity patterns may also change with task de-  
261 mands. For example, our brains may represent the same perceptual stimulus differently depending  
262 on which aspects of the stimulus or which combinations of features are task-relevant (Mack et al.,  
263 2020).

264 Different brain networks also varied in how informative and compressible their activity pat-  
265 terns were across experimental conditions (e.g., Fig. 4). This might follow from evolutionary  
266 optimizations that reflect the relevant constraints or demands placed on those networks. One  
267 possibility is that cortex is organized in a hierarchy of networks “concerned with” or selective to  
268 different levels of processing or function. To the extent that different levels of processing (e.g.,  
269 low-level sensory processing versus “deeper” higher-level processing) reflect different stimulus  
270 timescales (e.g., Manning, 2020), the network differences we observed might also relate to the  
271 timescales at which each network is maximally sensitive (Baldassano et al., 2017; Hasson et al.,  
272 2008; Lerner et al., 2011; Regev et al., 2018).

## 273 Concluding remarks

274 Cognitive neuroscientists are still grappling with basic questions about the fundamental “rules”  
275 describing how our brains respond, and about how brain activity patterns and the associated  
276 underlying cognitive representations and computations are linked. We identified two aspects of  
277 brain activity patterns, informativeness and compressibility, that appear to change systematically

278 with task demands and across brain networks. Our work helps to clarify how the “neural code”  
279 might be structured, and how the code might vary across tasks and brain areas.

280 **Methods**

281 We measured properties of recorded neuroimaging data under different task conditions that varied  
282 systematically in cognitive engagement and depth of processing. We were especially interested in  
283 how *informative* and *compressible* the activity patterns were under these different conditions (Fig. 1).

284 **Functional neuroimaging data collected during story listening**

285 We examined an fMRI dataset collected by Simony et al. (2016) that the authors have made publicly  
286 available at [arks.princeton.edu/ark:/88435/dsp015d86p269k](https://arks.princeton.edu/ark:/88435/dsp015d86p269k). The dataset comprises neuroimaging  
287 data collected as participants listened to an audio recording of a story (intact condition; 36 par-  
288 ticipants), listened to temporally scrambled recordings of the same story (17 participants in the  
289 paragraph-scrambled condition listened to the paragraphs in a randomized order and 36 in the  
290 word-scrambled condition listened to the words in a randomized order), or lay resting with their  
291 eyes open in the scanner (rest condition; 36 participants). Full neuroimaging details may be found  
292 in the original paper for which the data were collected (Simony et al., 2016). Procedures were  
293 approved by the Princeton University Committee on Activities Involving Human Subjects, and by  
294 the Western Institutional Review Board (Puyallup, WA). All subjects were native English speakers  
295 with normal hearing and provided written informed consent.

296 **Hierarchical topographic factor analysis (HTFA)**

297 Following our prior related work, we used HTFA (Manning et al., 2018) to derive a compact  
298 representation of the neuroimaging data. In brief, this approach approximates the timeseries  
299 of voxel activations (44,415 voxels) using a much smaller number of radial basis function (RBF)  
300 nodes (in this case, 700 nodes, as determined by an optimization procedure; Manning et al., 2018)).  
301 This provides a convenient representation for examining full-brain activity patterns and network  
302 dynamics. All of the analyses we carried out on the neuroimaging dataset were performed in

303 this lower-dimensional space. In other words, each participant's data matrix was a number-of-  
304 timepoints ( $T$ ) by 700 matrix of HTFA-derived factor weights (where the row and column labels  
305 were matched across participants). Code for carrying out HTFA on fMRI data may be found as  
306 part of the BrainIAK toolbox (Capota et al., 2017; Kumar et al., 2021), which may be downloaded  
307 at [brainiak.org](http://brainiak.org).

308 **Principal components analysis (PCA)**

309 We applied group PCA (Smith et al., 2014) separately to the HTFA-derived representations of the  
310 data (i.e., factor loadings) from each experimental condition. Specifically, for each condition, we  
311 considered the set of all participants'  $T$  by 700 factor weight matrices. We used group PCA to project  
312 these 700-dimensional matrices into a series of shared  $k$ -dimensional spaces, for  $k \in \{3, 4, 5, \dots, 700\}$ .  
313 This yielded a set of number-of-participants matrices, each with  $T$  rows and  $k$  columns.

314 **Temporal decoding**

315 We sought to identify neural patterns that reflected participants' ongoing cognitive processing of  
316 incoming stimulus information. As reviewed by Simony et al. (2016), one way of homing in on  
317 these stimulus-driven neural patterns is to compare activity patterns across individuals. In partic-  
318 ular, neural patterns will be similar across individuals to the extent that the neural patterns under  
319 consideration are stimulus-driven, and to the extent that the corresponding cognitive representa-  
320 tions are reflected in similar spatial patterns across people (Simony & Chang, 2020). Following this  
321 logic, we used an across-participant temporal decoding test developed by Manning et al. (2018) to  
322 assess the degree to which different neural patterns reflected ongoing stimulus-driven cognitive  
323 processing across people. The approach entails using a subset of the data to train a classifier to  
324 decode stimulus timepoints (i.e., moments in the story participants listened to) from neural pat-  
325 terns. We use decoding (forward inference) accuracy on held-out data, from held-out participants,  
326 as a proxy for the extent to which the inputted neural patterns reflected stimulus-driven cognitive  
327 processing in a similar way across individuals.

328 **Forward inference and decoding accuracy**

329 We used an across-participant correlation-based classifier to decode which stimulus timepoint  
330 matched each timepoint's neural pattern. For a given value of  $k$  (i.e., number of principal compo-  
331 nents), we first used group PCA to project the data from each condition into a shared  $k$ -dimensional  
332 space. Next, we divided the participants into two groups: a template group,  $\mathcal{G}_{\text{template}}$  (i.e., training  
333 data), and a to-be-decoded group,  $\mathcal{G}_{\text{decode}}$  (i.e., test data). We averaged the projected data within  
334 each group to obtain a single  $T$  by  $k$  matrix for each group. Next, we correlated the rows of the two  
335 averaged matrices to form a  $T$  by  $T$  decoding matrix,  $\Lambda$ . In this way, the rows of  $\Lambda$  reflected time-  
336 points from the template group, while the columns reflected timepoints from the to-be-decoded  
337 group. We used  $\Lambda$  to assign temporal labels to each timepoint (row) from the test group's ma-  
338 trix, using the row of the training group's matrix with which it was most highly correlated. We  
339 repeated this decoding procedure, but using  $\mathcal{G}_{\text{decode}}$  as the template group and  $\mathcal{G}_{\text{template}}$  as the  
340 to-be-decoded group. Given the true timepoint labels (for each group), we defined the decoding  
341 accuracy as the average proportion of correctly decoded timepoints, across both groups (where  
342 chance performance is  $\frac{1}{T}$ ). In Figures 2 and 3 we report the decoding accuracy for each condition  
343 and value of  $k$ , averaged across  $n = 100$  cross validation folds.

344 **Reverse inference**

345 To help interpret the brain activity patterns we found within the contexts of other studies, we  
346 created summary maps of each principal component, for each experimental condition, by summing  
347 together the 20 HTFA-derived RBF nodes (see *Hierarchical Topographic Factor Analysis*) with the  
348 highest absolute value weights for each of the top 5 components (Figs. 5, S1). We then carried  
349 out a meta analysis using Neurosynth (Rubin et al., 2017) to identify the 5 terms most commonly  
350 associated with the given map.

351 **Data and code availability**

352 All of the code used to produce the figures and results in this manuscript, along with links to the  
353 corresponding data, may be found at [github.com/ContextLab/pca\\_paper](https://github.com/ContextLab/pca_paper).

354 **Acknowledgements**

355 We acknowledge discussions with Rick Betzel, Luke Chang, Emily Finn, and Jim Haxby. Our  
356 work was supported in part by NSF CAREER Award Number 2145172 to J.R.M. The content is  
357 solely the responsibility of the authors and does not necessarily represent the official views of our  
358 supporting organizations. The funders had no role in study design, data collection and analysis,  
359 decision to publish, or preparation of the manuscript.

360 **Author contributions**

361 Conceptualization: J.R.M. and L.L.W.O. Methodology: J.R.M. and L.L.W.O. Implementation: L.L.W.O.  
362 Analysis: L.L.W.O. Writing, Reviewing, and Editing: J.R.M. and L.L.W.O. Supervision: J.R.M.

363 **References**

- 364 Adachi, Y., Osada, T., Sporns, O., Watanabe, T., Matsui, T., Miyamoto, K., & Miyashita, Y.  
365 (2012). Functional connectivity between anatomically unconnected areas is shaped by collective  
366 network-level effects in the macaque cortex. *Cerebral Cortex*, 22(7), 1586–1592.
- 367 Alvarez, S. A. (2002). *An exact analytical relation among recall, precision, and classification accuracy in*  
368 *information retrieval* (Technical Report No. BCCS-02-01). Boston College.
- 369 Baldassano, C., Chen, J., Zadbood, A., Pillow, J. W., Hasson, U., & Norman, K. A. (2017). Discov-  
370 ering event structure in continuous narrative perception and memory. *Neuron*, 95(3), 709–721.
- 371 Bassett, D. S., & Sporns, O. (2017). Network neuroscience. *Nature Neuroscience*, 20(3), 353–364.
- 372 Brovelli, A., Ding, M., Ledberg, A., Chen, Y., Nakamura, R., & Bressler, S. (2004). Beta oscillations in  
373 a large-scale sensorimotor cortical network: directional influences revealed by Granger causality.  
374 *Proceedings of the National Academy of Sciences, USA*, 101(26), 9849–9854.
- 375 Bullmore, E., & Sporns, O. (2009). Complex brain networks: graph theoretical analysis of structural  
376 and functional systems. *Nature Reviews Neuroscience*, 10(3), 186–198.

- 377 Capota, M., Turek, J., Chen, P.-H., Zhu, X., Manning, J. R., Sundaram, N., ... Shin, Y. S. (2017).  
378     *Brain imaging analysis kit.*
- 379 Cole, M. W., Bassett, D. S., Power, J. D., Braver, T. S., & Petersen, S. E. (2014). Intrinsic and  
380     task-evoked network architectures of the human brain. *Neuron*, 83(1), 238–251.
- 381 Dhamala, M., Rangarajan, G., & Ding, M. (2008). Analyzing information flow in brain networks  
382     with nonparametric Granger causality. *NeuroImage*, 41(2), 354–362.
- 383 Finn, E. S., Scheinost, D., Finn, D. M., Shen, X., Papademetris, X., & Constable, R. T. (2017).  
384     Can brain state be manipulated to emphasize individual differences in functional connectivity.  
385     *NeuroImage*, 160, 140–151.
- 386 Finn, E. S., Shen, X., Scheinost, D., Rosenberg, M. D., Huang, J., Chun, M. M., ... Constable, R. T.  
387     (2015). Functional connectome fingerprinting: identifying individuals using patterns of brain  
388     connectivity. *Nature Neuroscience*, 18, 1664–1671.
- 389 Glerean, E., Salmi, J., Lahnakoski, J. M., Jääskeläinen, I. P., & Sams, M. (2012). Functional magnetic  
390     resonance imaging phase synchronization as a measure of dynamic functional connectivity.  
391     *Brain Connectivity*, 2(2), 91–101.
- 392 Gratton, C., Laumann, T. O., Nielsen, A. N., Greene, D. J., Gordon, E. M., Gilmore, A. W., ...  
393 Petersen, S. E. (2018). Functional brain networks are dominated by stable group and individual  
394     factors, not cognitive or daily variation. *Neuron*, 98(2), 439–452.
- 395 Hasson, U., Yang, E., Vallines, I., Heeger, D. J., & Rubin, N. (2008). A hierarchy of temporal  
396     receptive windows in human cortex. *The Journal of Neuroscience*, 28(10), 2539–2550.
- 397 Korzeniewska, A., Crainiceanu, C. M., Kus, R., Franaszczuk, P. J., & Crone, N. E. (2008). Dynamics  
398     of event-related causality in brain electrical activity. *Human Brain Mapping*, 29(10).
- 399 Kumar, M., Anderson, M. J., Antony, J. W., Baldassano, C., Brooks, P. P., Cai, M. B., ... Norman,  
400     K. A. (2021). BrainIAK: the brain image analysis kit. *Aperture*, *In press*.
- 401 Lerner, Y., Honey, C. J., Silbert, L. J., & Hasson, U. (2011). Topographic mapping of a hierarchy of  
402     temporal receptive windows using a narrated story. *The Journal of Neuroscience*, 31(8), 2906–2915.

- 403 Mack, M. L., Preston, A. R., & Love, B. C. (2020). Ventromedial prefrontal cortex compressesion  
404 during concept learning. *Nature Communications*, 11(46), doi.org/10.1038/s41467-019-13930-8.
- 405 Manning, J. R. (2020). Context reinstatement. In M. J. Kahana & A. D. Wagner (Eds.), *Handbook of*  
406 *human memory*. Oxford University Press.
- 407 Manning, J. R., Zhu, X., Willke, T. L., Ranganath, R., Stachenfeld, K., Hasson, U., ... Norman,  
408 K. A. (2018). A probabilistic approach to discovering dynamic full-brain functional connectivity  
409 patterns. *NeuroImage*, 180, 243–252.
- 410 Norman, K. A., Polyn, S. M., Detre, G. J., & Haxby, J. V. (2006). Beyond mind-reading: multi-voxel  
411 pattern analysis of fMRI data. *Trends in Cognitive Sciences*, 10(9), 424–430.
- 412 Owen, L. L. W., Chang, T. H., & Manning, J. R. (2021). High-level cognition during story listening is  
413 reflected in high-order dynamic correlations in neural activity patterns. *Nature Communications*,  
414 12(5728), doi.org/10.1038/s41467-021-25876-x.
- 415 Owen, L. L. W., Muntianu, T. A., Heusser, A. C., Daly, P., Scangos, K. W., & Manning, J. R. (2020). A  
416 Gaussian process model of human electrocorticographic data. *Cerebral Cortex*, 30(10), 5333–5345.
- 417 Preti, M. G., Bolton, T. A. W., & Van De Ville, D. (2017). The dynamic functional connectome:  
418 state-of-the-art and perspectives. *NeuroImage*, 160, 41–54.
- 419 Regev, M., Simony, E., Lee, K., Tan, K. M., Chen, J., & Hasson, U. (2018). Propagation of information  
420 along the cortical hierarchy as a function of attention while reading and listening to stories.  
421 *Cerebral Cortex*.
- 422 Rogers, B. P., Morgan, V. L., Newton, A. T., & Gore, J. C. (2007). Assessing functional connectivity  
423 in the human brain by fMRI. *Magnetic Resonance Imaging*, 25(11), 1347–1357.
- 424 Rubin, T. N., Kyoejo, O., Gorgolewski, K. J., Jones, M. N., Poldrack, R. A., & Yarkoni, T. (2017).  
425 Decoding brain activity using a large-scale probabilistic functional-anatomical atlas of human  
426 cognition. *PLoS Computational Biology*, 13(10), e1005649.
- 427 Rubinov, M., & Sporns, O. (2010). Complex network measures of brain connectivity: uses and  
428 interpretations. *NeuroImage*, 52, 1059–1069.

- 429 Scangos, K. W., Khambhati, A. N., Daly, P. M., Owen, L. L. W., Manning, J. R., Ambrose, J. B.,  
430 ... Chang, E. F. (2021). Biomarkers of depression symptoms defined by direct intracranial  
431 neurophysiology. *Frontiers in Human Neuroscience*, In press.
- 432 Shannon, C. E. (1948). A mathematical theory of communication. *Bell System Technical Journal*,  
433 27(3), 379–423.
- 434 Simony, E., & Chang, C. (2020). Analysis of stimulus-induced brain dynamics during naturalistic  
435 paradigms. *NeuroImage*, 216, 116461.
- 436 Simony, E., Honey, C. J., Chen, J., & Hasson, U. (2016). Dynamic reconfiguration of the default  
437 mode network during narrative comprehension. *Nature Communications*, 7(12141), 1–13.
- 438 Sizemore, A. E., Giusti, C., Kahn, A., Vettel, J. M., Betzel, R. F., & Bassett, D. S. (2018). Cliques and  
439 cavities in the human connectome. *Journal of Computational Neuroscience*, 44(1), 115–145.
- 440 Smith, S. M., Beckmann, C. F., Andersson, J., Auerbach, E. J., Bijsterbosch, J., Douaud, G., ...  
441 Glasser, M. F. (2013). Resting-state fMRI in the Human Connectome Project. *NeuroImage*, 80,  
442 144–168.
- 443 Smith, S. M., Fox, P. T., Miller, K. L., Glahn, D. C., Fox, P. M., Mackay, C. E., ... Beckmann,  
444 C. F. (2009). Correspondence of the brain's functional architecture during activation and rest.  
445 *Proceedings of the National Academy of Sciences, USA*, 106(31), 13040–13045.
- 446 Smith, S. M., Hyvärinen, A., Varoquaux, G., Miller, K. L., & Beckmann, C. F. (2014). Group-PCA  
447 for very large fMRI datasets. *NeuroImage*, 101, 738–749.
- 448 Smith, S. M., Vidaurre, D., Beckmann, C. F., Glasser, M. F., Jenkinson, M., Miller, K. L., ... Van  
449 Essen, D. C. (2013). Functional connectomics from resting-state fMRI. *Trends in Cognitive Sciences*,  
450 17(12), 666–682.
- 451 Sporns, O., & Betzel, R. F. (2016). Modular brain networks. *Annual Review of Psychology*, 67,  
452 613–640.
- 453 Sporns, O., & Honey, C. J. (2006). Small worlds inside big brains. *Proceedings of the National Academy  
454 of Sciences, USA*, 103(51), 19219–19220.

- 455 Sporns, O., & Zwi, J. D. (2004). The small world of the cerebral cortex. *Neuroinformatics*, 2(2),  
456 145–162.
- 457 Srinivasan, R., Winter, W. R., Ding, J., & Nunez, P. L. (2007). EEG and MEG coherence: Measures of  
458 functional connectivity at distinct spatial scales of neocortical dynamics. *Journal of Neuroscience  
459 Methods*, 166, 41–52.
- 460 Tomasi, D., & Volkow, N. D. (2011). Association between functional connectivity hubs and brain  
461 networks. *Cerebral Cortex*, 21, 2003–2013.
- 462 Yeo, B. T. T., Krienen, F. M., Sepulcre, J., Sabuncu, M. R., Lashkari, D., Hollinshead, M., . . . Buckner,  
463 R. L. (2011). The organization of the human cerebral cortex estimated by intrinsic functional  
464 connectivity. *Journal of Neurophysiology*, 106(3), 1125–1165.